

# SIMULATING ULTRACOLD ATOMS

CHRISTOPHER JON WATKINS



From classical to quantum gases

December 2013 – version 0.0.1

Christopher Jon Watkins: *Simulating Ultracold Atoms*, From classical to quantum gases, © December 2013

Ohana means family.  
Family means nobody gets left behind, or forgotten.  
— Lilo & Stitch

Dedicated to the loving memory of Rudolf Miede.  
1939–2005



## ABSTRACT

---

Short summary of the contents...



## PUBLICATIONS

---

Some ideas and figures have appeared previously in the following publications:

Put your publications from the thesis here. The packages `multibib` or `bibtopic` etc. can be used to handle multiple different bibliographies in your document.





*We have seen that computer programming is an art,  
because it applies accumulated knowledge to the world,  
because it requires skill and ingenuity, and especially  
because it produces objects of beauty.*

— ? [? ]

## ACKNOWLEDGEMENTS

---

Put your acknowledgements here.

Many thanks to everybody who already sent me a postcard!

Regarding the typography and other help, many thanks go to Marco Kuhlmann, Philipp Lehman, Lothar Schlesier, Jim Young, Lorenzo Pantieri and Enrico Gregorio<sup>1</sup>, Jörg Sommer, Joachim Köstler, Daniel Gottschlag, Denis Aydin, Paride Legovini, Steffen Prochnow, Nicolas Repp, Hinrich Harms, Roland Winkler, and the whole L<sup>A</sup>T<sub>E</sub>X-community for support, ideas and some great software.

Regarding L<sup>y</sup>X: The L<sup>y</sup>X port was initially done by Nicholas Mariette in March 2009 and continued by Ivo Pletikosić in 2011. Thank you very much for your work and the contributions to the original style.

---

<sup>1</sup> Members of GuIT (Gruppo Italiano Utilizzatori di T<sub>E</sub>X e L<sup>A</sup>T<sub>E</sub>X)



## CONTENTS

---

<b>i</b>	<b>INTRO MATERIAL</b>	<b>1</b>
1	INTRODUCTION	3
1.1	Magnetic Trapping . . . . .	3
<b>ii</b>	<b>DSMC</b>	<b>5</b>
2	SIMULATING COLLISIONS IN THERMAL GASES	7
2.1	Collision Rates in Thermal Gases . . . . .	7
2.2	DSMC simulations of collisions . . . . .	9
2.3	Thermalisation . . . . .	10
2.3.1	Walraven Thermalisation . . . . .	10
2.3.2	Monroe Thermalisation . . . . .	12
2.4	Evaporation . . . . .	13
2.5	DSMC simulations of Evaporation . . . . .	14
2.6	Adiabaticity . . . . .	14
3	MAJORANA INTERLUDE	17
3.1	Majornan Spin Flips . . . . .	17
3.2	Landau Zener Formula . . . . .	17
3.3	Loss Rates 'n' Stuff . . . . .	17
4	DSMC WITH SPIN - EHRENFEST	19
4.1	Simulating Schrödinger Equation . . . . .	19
4.2	Schrödinger Simulations . . . . .	20
4.3	Single Atom Spin Flips . . . . .	22
4.4	Full Gas Simulations . . . . .	23
4.4.1	Ioffe Pritchard Trap . . . . .	24
4.4.2	Quadrupole Trap . . . . .	25
5	DSMC WITH SPIN - MCWF	27
5.1	Single Atom Spin Flips . . . . .	27
5.2	Full Gas Simulations . . . . .	28
5.2.1	Ioffe Pritchard Trap . . . . .	29
5.2.2	Quadrupole Trap . . . . .	29
<b>iii</b>	<b>FEMDVR</b>	<b>31</b>
6	FEMDVR	33
6.1	1D FEMDVR . . . . .	33
6.1.1	Scaling Comparison to CPU . . . . .	33
6.1.2	Real Simulation . . . . .	33
6.2	3D FEMDVR . . . . .	33
6.2.1	Knots . . . . .	33
<b>iv</b>	<b>CUDA</b>	<b>35</b>
7	CUDA DSMC	37
7.1	CUDA . . . . .	37

7.1.1	Parallelisation . . . . .	37
7.2	Speed up . . . . .	37
7.2.1	Some simulations . . . . .	37
V	APPENDIX	39
A	THERMAL PHYSICS	41
A.1	Collision Rates in Thermal Gases . . . . .	41
A.2	Thermalisation . . . . .	41
A.2.1	Walraven Thermalisation . . . . .	41
B	MAGNETIC TRAPPING	43
C	MOTION INTEGRATION	45
C.1	Euler Method . . . . .	45
C.2	Semi-Implicit Euler Method . . . . .	45
C.3	Verlet Algorithm . . . . .	45
C.4	Leap Frog Method . . . . .	46
C.5	Velocity Verlet . . . . .	46
C.6	Beeman's Algorithm . . . . .	46
D	DIRECT SIMULATION MONTE CARLO	47
D.1	Appendix Section Test . . . . .	47
D.2	Another Appendix Section Test . . . . .	48
E	NON-DIMENSIONALISATION	49
E.1	Quasi - 1D GPE . . . . .	49
E.2	Majorana Problem Spin Half . . . . .	51
E.3	Another Appendix Section Test . . . . .	52
F	FINITE ELEMENT METHOD	53
	BIBLIOGRAPHY	55

## LIST OF FIGURES

---

Figure 2.1	Error of DSMC method as a function of test particle number and cell number. . . . .	9
Figure 2.2	Walraven rethermalisation. I want to do this simulation for some different perturbation temperatures. One more higher and one lower too. . . . .	11
Figure 2.3	Walraven rethermalisation. I want to do this simulation for some different perturbation temperatures. One more higher and one lower too. . . . .	12
Figure 4.1	Simulating the no majorana spin flip . . . . .	21
Figure 4.2	No flip and flip in the same simulation. . . . .	23
Figure 4.3	Ehrenfest method for a gas in an IP trap. . . . .	24
Figure 5.1	No flip and flip in the same simulation mcwf. . . .	27

## LIST OF TABLES

---

Table 2.1	Collision rates for different trapping potentials. . .	8
Table D.1	Autem usu id . . . . .	48
Table E.1	Autem usu id . . . . .	52

## LISTINGS

---

Listing 4.1	Psuedo-code algorithm for a single Ehrenfest method time step . . . . .	22
Listing D.1	A floating example . . . . .	48
Listing E.1	A floating example . . . . .	52

## ACRONYMS

---

DRY Don't Repeat Yourself

API Application Programming Interface

UML Unified Modeling Language



## Part I

### INTRO MATERIAL

You can put some informational part preamble text here. Illo principalmente su nos. Non message occidental angloromanic da. Debitas effortio simplicate sia se, auxiliar summarios da que, se avantiate publicationes via. Pan in terra summarios, capital interlingua se que. Al via multo esser specimen, campo responder que da. Le usate medical addresses pro, europa origine sanctificate nos se.



## INTRODUCTION

---

I am going to need to introduce the different trapping potentials in here some where I think.

### 1.1 MAGNETIC TRAPPING

Ioffe Pritchard trap

$$\mathbf{B}_{\text{IP}}(x, y, z) = B_0 \begin{bmatrix} 0 \\ 0 \\ 0 \end{bmatrix} + B' \begin{bmatrix} x \\ -y \\ 0 \end{bmatrix} + \frac{1}{2} B'' \begin{bmatrix} -xz \\ -yz \\ z^2 - \frac{1}{2}(x^2 + y^2) \end{bmatrix} \quad (1.1)$$

the magnitude of this field can be approximated as the following for small position

$$|\mathbf{B}_{\text{IP}}| = \frac{1}{2} (B''_\rho (x^2 + y^2) + B'' z^2), \quad (1.2)$$

where

$$B''_\rho = \frac{B'^2}{B_0} - \frac{B''}{2}.$$

Quadrupole trap

$$\mathbf{B}_{\text{Q}}(x, y, z) = \frac{1}{2} B_z \begin{bmatrix} x \\ y \\ -2z \end{bmatrix} \quad (1.3)$$



## Part II

### DSMC

You can put some informational part preamble text here. Illo principalmente su nos. Non message occidental angloromanic da. Debitas effortio simplicate sia se, auxiliar summarios da que, se avantiate publicationes via. Pan in terra summarios, capital interlingua se que. Al via multo esser specimen, campo responder que da. Le usate medical addresses pro, europa origine sanctificate nos se.



## SIMULATING COLLISIONS IN THERMAL GASES

---

Need to introduce the usefulness of the method here. References to many kinds of applications and such things. I also need to perform a literature review of all DSMC used in cold atoms physics.

Compare to molecular dynamic approaches, when is DSMC appropriate / good? When does it fail?

Find out the knudsen number for typical cold atom conditions. Wade has numbers for stamper kern and shvatchuck.

DSMC - Birds Book [1]

Evaporative Cooling and Expansion Dynamics: [2–4]

Bosonic Collective-Mode dynamics: [5–9], Can't find Jackson Zaremba 2002 Laser Physics, 12, 93

Fermion Dynamics: [10–13] (see also [14–17])

Sympathetic Cooling: [18, 19]

Applications - Rayleigh Bernard Flow: [20]

Spacecraft aerodynamics: [21]

Chemical reactions: [22] Goldsworthy?

Microfluidics: [23]

Acoustics on Earth, Mars and Titan: [24]

Volcanic plumes on Jupiter: [25]

Read: [26], [45]

Refer to cuda section 7 Should also discuss the development of this parallel implementation of the code. Compare to CPU implementations. Goldsworthy has a few references for other CUDA codes.

The heart of the DSMC method is to simplify the simulation of inter-particle interactions in the form of two body collisions. In this sense there are two aspects we need to ensure are modelled accurately; the number and frequency of collisions (collision rate) and the collisions themselves, whether or not they are correctly distributing the kinetic energy. In the following sections I carefully analyse these two aspects to ensure the utmost accuracy in our simulations.

### 2.1 COLLISION RATES IN THERMAL GASES

Overall collision rate, spatial collision rate, talk about number of cells, the occupancy of cells and the effect of inhomogeneity.

One of the most basic tests of the application of the DSMC method to cold atom physics is to investigate the collision rate for a thermal gas. Using the Boltzmann equation we can derive [27] the thermally averaged

*Maybe say something about the Boltzmann equation here and give some references.*

TRAPPING POTENTIAL	TRAP POWER	EFFECTIVE VOLUME, $V_e$	COLLISION RATE, $\tau_c^{-1}$
Homogeneous Gas	$\infty?$	$V$	$\frac{1}{2^{1/2}} n_0 \bar{v} \sigma$
Spherical Quadrupole	1	$256\pi \left( \frac{k_B T}{g_s \mu_B B_z} \right)^3$	$\frac{1}{2^{7/2}} n_0 \bar{v} \sigma$
Ioffe Pritchard	2	$\frac{8}{\sqrt{B'' B''_\rho}} \left( \frac{\pi k_B T}{g_s \mu_B} \right)^{3/2}$	$\frac{1}{2^2} n_0 \bar{v} \sigma$
Isotropic Power Law	$3/\gamma$	$\frac{4}{3} \pi r_e^3 \Gamma[\gamma + 1] \left( \frac{k_B T}{\mathcal{U}_0} \right)^\gamma$	$\frac{1}{2^{\gamma+0.5}} n_0 \bar{v} \sigma$

Table 2.1: Collision rates for different trapping potentials.

collision rate per unit density for a single species atomic gas bound by the potential  $\mathcal{U}(\mathbf{r})$ ,

$$\tau_c^{-1} = \frac{1}{2} n_0 \langle v \sigma \rangle \frac{V_{2e}}{V_e}, \quad (2.1)$$

where  $n_0 = N/V_e$  is the central density of the gas,  $\langle v \sigma \rangle$  is the thermally averaged product of the atomic velocity and collision cross section,  $V_e = \int \exp[-\mathcal{U}(\mathbf{r})/k_B T] d\mathbf{r}$  is the effective volume of the gas, and  $V_{2e} = \int \exp[-2\mathcal{U}(\mathbf{r})/k_B T] d\mathbf{r}$  the effective volume corresponding to the distribution of pairs. For the bulk of this work we will consider collisions in three unique trapping potentials: no trapping potential, i. e. a homogeneous gas, an Ioffe Pritchard trap(cite) and a spherical quadrupole trap(cite - is it really spherical?)<sup>1</sup>. In table 2.1 we have derived the expressions for the effective volume and average collision rates for each of these traps. We have also included the results for a general isotropic power law trap, the potential of which is described by

$$\mathcal{U}_{PL}(\mathbf{r}) = \mathcal{U}_0 \left( \frac{r}{r_e} \right)^{3/\gamma}, \quad (2.2)$$

where the trap has a characteristic trap size  $r_e$  and a trap strength of  $\mathcal{U}_0$ . The parameter,  $\bar{v}$ , in table 2.1 is the thermally averaged atomic speed and is given by

$$\bar{v} = \sqrt{\frac{8k_B T}{\pi m}}.$$

We can make a few interesting observations from these calculations. The most interesting is that the collision rate in the trapped gases increases as the temperature decreases, which is the converse to the homogeneous gas<sup>2</sup>. This is because for a trapped gas the central density increases at a rate greater than the decrease of the average thermal velocity,  $\bar{v}$ . For the homogeneous gas the density remains constant as the gas cools, thus the

<sup>1</sup> We have a more in depth discussion of magnetic trapping in appendix B.

<sup>2</sup> This relationship between collision rate and temperature for trapped gases is what gives rise to the "runaway" evaporation observed during atom cooling experiments.



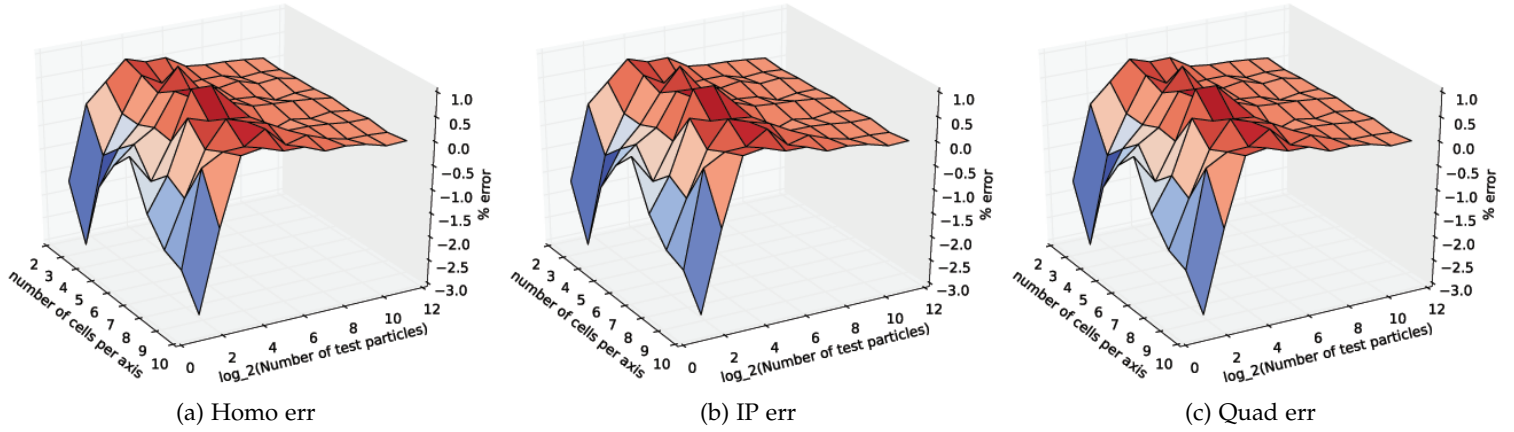


Figure 2.1: Error of DSMC method as a function of test particle number and cell number.

decrease in the velocity of the atoms results in an overall decrease in the collision rate. We can also see that if we can hold the trap strength and effective trap size constant the central density of the trap will increase as the power of the trap decrease (or as  $\gamma$  increases). This is often spoken about in terms of "tightness" and is a strong motivator behind the use of the quadrupole trap. In section 2.4 we will show that it is the tightness of a trap that determines it's efficiency in evaporative cooling.

## 2.2 DSMC SIMULATIONS OF COLLISIONS

The DSMC method offers some free parameters which we can optimise to balance the accuracy and efficiency of the algorithm, namely the number of cells,  $n_c$ , and the number of test particles,  $N_p$ . We wish to see the effect of varying these parameters on the results of the simulation.

\*\*Include a surface plot of the collision rate as a function of cell number and test particle number. Should make the z axis percentage error. See fig 14. in wade. \*\*

Figure 2.5a shows how well the DSMC method performs over a wide range of test particle and cell numbers in a homogeneous gas. We can see in the corner the method beginning to fail. This is the region where, on average, we have less than two test particles per cell. This means that there is not enough atoms to perform a collision within a cell. One way to avoid this (which has not been implemented here) is to search neighbouring cells for collision pairs when a partner can not be found in the current cell. The main thing to observe here is the increase in the error as the number of test particles is reduced.

Smaller cells -> larger fluctuations.

Not adaptive since slowly changing cloud.

### 2.3 THERMALISATION

Once we are convinced that we have the correct number of collisions we must confirm that they are performing as they should. The perfect way to test this is through the investigation of thermal relaxation or the process of thermalisation through elastic collisions. There are many ways that a system can be out of equilibrium, but here we will investigate three scenarios from the literature that have a concrete theoretical backing to which we can compare our simulations.

*Thermalisation is the generic name for all kinds of processes giving rise to relaxation towards thermal equilibrium starting from a non-equilibrium situation. \*\*REWORD, NOT MY WORDS\*\**

#### 2.3.1 Walraven Thermalisation

The simplest example for rethermalisation is somewhat reminiscent of evaporative cooling, that is the case is simply perturbing the equilibrium by adding a small number of atoms whose average energy is different to that of the bulk gas. In [27] (the analysis of which we step through in detail in appendix A.2.1) we are shown that the rethermalisation time,  $\tau_{\text{th}}^{-1}$ , is given by

$$\tau_{\text{th}}^{-1} = \frac{1}{2(\gamma + 3/2)} \tau_{\text{c}}^{-1}. \quad (2.3)$$

If we use the values for the trapping parameter,  $\gamma$ , given in table 2.1 we would expect the thermalisation time in a homogeneous, IP and quadrupole trap to be 3, 6 and 9 times the collision time in each trap respectively. Anderlini and Guéry-Odelin [28] have taken this analysis one step further, considering the effect including all partial waves in the collision integrals has on a homogeneous box trap and a harmonic potential. Interestingly in the limit of constant cross section the results for the homogeneous trap reduces to that given in equation (2.3) with  $\gamma = 0$ . In fact they go on to show that for the harmonic trap the thermalisation time is longer by a factor of 2, which again, agrees with equation (2.3) with  $\gamma = 3/2$ .

Before we consider these simulations numerically the reader might be a little confused by the above result. Looking at equation 2.3 it is quite clear that as the trapping parameter,  $\gamma$ , increases the number of collision required for thermalisation increases. This might be a little counter intuitive. We just stated in section 2.1 that evaporative cooling, a process driven by rethermalisation is more efficient in tighter trapping potentials i.e. larger trapping parameters. Anderlini et al. explain this best when they say

...the fact that the space of configuration is larger for a non-homogeneous gas, and that the thermalization affects both the space and velocity degrees of freedom.

We can understand this better if we consider an effective volume in configuration space,  $V_{\text{cs}}$ , (analogous to the effective volume in real space,  $V_{\text{e}}$ )

$$V_{\text{cs}} = \int \exp \left[ -\frac{H(\mathbf{r}, \mathbf{v})}{k_{\text{B}} T} \right] d\mathbf{r} d\mathbf{v} = V_{\text{e}} \left( \frac{3\pi m}{k_{\text{B}} T} \right)^{3/2}. \quad (2.4)$$

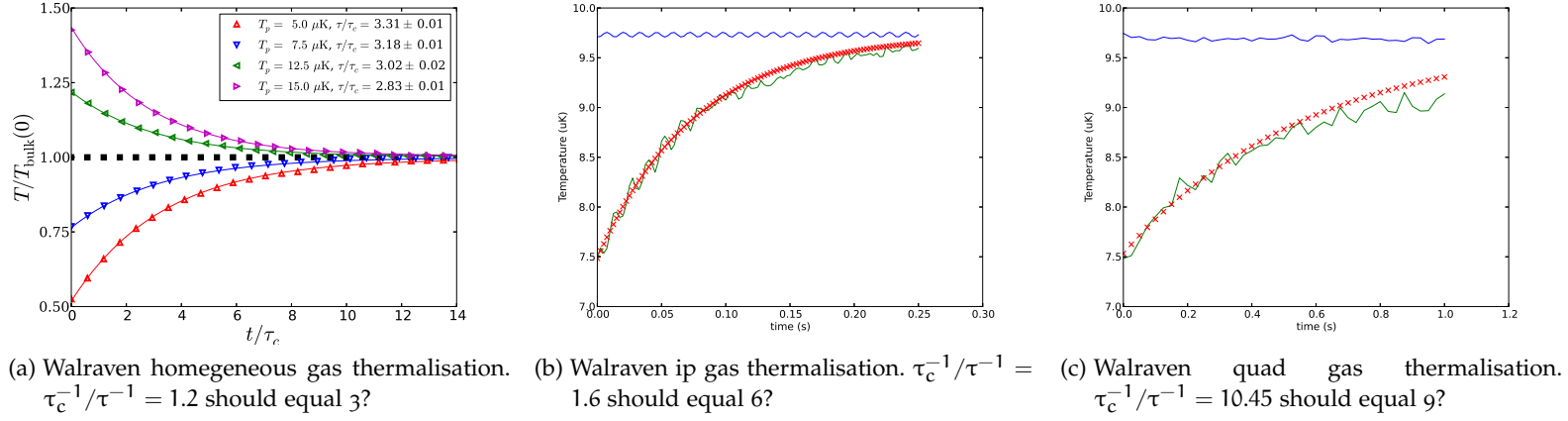


Figure 2.2: Walraven rethermalisation. I want to do this simulation for some different perturbation temperatures. One more higher and one lower too.

So we can see that for a given temperature the region occupied in configuration space increases with the effective volume, which table 2.1 shows increases with  $\gamma$ . Again this might make the reader uncomfortable, we seem to have convincingly shown that tighter trapping potentials take longer to thermalise. However, even though the number of collisions required to thermalise the gas increases with the trapping parameter,  $\gamma$ , the average time between collisions,  $\tau_c$ , decreases. Thus the absolute time required for a gas to thermalise is lower for tighter trapping potentials i.e. larger  $\gamma$ .

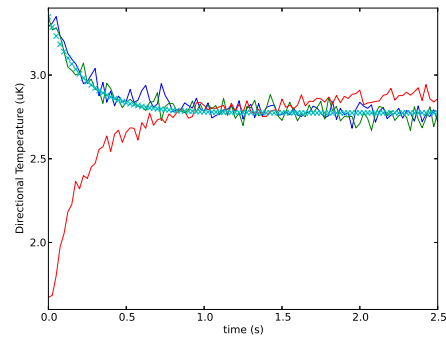
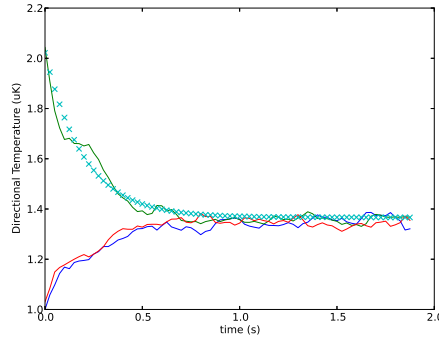
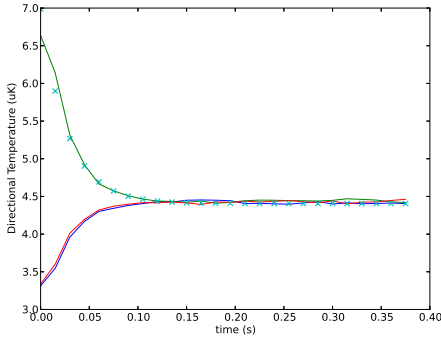
In figure 2.2 we have simulated a million physical atoms,  $N_P = 10^6$ , at 10  $\mu\text{K}$  in three different trapping potentials: homogeneous, IP and quadrupole. Each gas began in an initially thermal distribution with 10% of the particles at set to have an average temperature of 12.5  $\mu\text{K}$ . For each simulation we have chosen the trapping parameters such that the collision rate was approximately 25 collisions per atom per second, as this number is similar to atoms of this temperature in an evaporation experiment. We used one million test particle,  $N_T = 10^6$ , in each simulation so that the ratio of physical atoms to test particles was one,  $\alpha = 1$ .

For the homogeneous gas simulation shown in figure 2.2a I set the width of the box containing the atoms to be 100  $\mu\text{m}$  in each direction. This corresponds to a collision rate of 24.64  $\text{s}^{-1}$ . I found the thermalisation occurred in  $3.14 \pm 0.02$  collision times, closely resembling the result in equation (2.3).

For the Ioffe Pritchard trap simulation shown in figure 2.2b we set  $B_0 = 0.01 \text{ T}$ ,  $B' = 33.54 \text{ Tm}^{-1}$  and  $B'' = 75,000 \text{ Tm}^{-2}$  which equates to a  $B_\rho'' = 75,000 \text{ Tm}^{-2}$ . Choosing these trapping parameters gives a collision rate of 24.72  $\text{s}^{-1}$ . I found the thermalisation occurred in  $6 \pm 0.1$  collision times, again, in perfect agreement with equation (2.3).

Finally in the quadrupole trap simulation shown in figure 2.2c we set  $B_z = 2.8 \text{ Tm}^{-1}$  resulting in a collision rate of 25.48  $\text{s}^{-1}$ . I found the thermalisation occurred in  $9 \pm 0.1$  collision times, again, in perfect agreement with equation (2.3).

When choosing the initial perturbed distribution we must keep in mind the virial theorem [1]. The key result here is that in a thermal distribution we have  $\langle E_p \rangle = \frac{2\gamma}{3} \langle E_k \rangle = \gamma k_B T$ . So when choosing the width for the spatial distribution we must keep in mind the effective power of the trapping potential.



(a) Monroe homogeneous gas thermalisation.  
 $\tau_c^{-1}/\tau^{-1} = 0.77$

(b) Walraven homogeneous gas thermalisation.  
 $\tau_c^{-1}/\tau^{-1} = 2.21$

(c) Walraven quad gas thermalisation.  
 $\tau_c^{-1}/\tau^{-1} = 6.09$

Figure 2.3: Walraven rethermalisation. I want to do this simulation for some different perturbation temperatures. One more higher and one lower too.

We can note from all simulations shown in figure 2.2 that the thermalisation time appears to be independent of the size of the perturbation.

### 2.3.2 Monroe Thermalisation

Another interesting experiment that has been investigated in some depth is the rethermalisation of a directional anisotropy. In these experiments the kinetic energy is changed in one cartesian direction only (the spatial distribution is reshaped accordingly), creating a directional anisotropy in the distribution. This squeezed distribution is then allowed to rethermalise through elastic collisions. The original theoretical development of Myatt [29] predicts that in an harmonic trap the thermalisation time for a directional anisotropy is approximately 2.7. This result has been used to experimentally determine the collision cross section,  $\sigma$ , of atoms in ultra-cold gas experiments [30, 31]. This simulation has also been repeated by Wu and Foot [2] using the DSMC method. Here I have extended this investigation to consider the thermalisation times in our three favourite trapping potentials: homogeneous, Ioffe Pritchard and quadrupole. As we saw in section 2.3.1 we can't expect the thermalisation time to be the same in different trapping potentials. In fact, if the perturbation is kept the same, it was purely a function of the trapping parameter,  $\gamma$ .

Also do it for different temperatures or trap numbers.

\*\*\* MUST REDO ALL OF THESE SIMULATIONS WITH COLLISIONS WORKING CORRECTLY (I.E. WITH THE NEW SORTING FIX IMPLEMENTED). \*\*\*

*Comment on directional temperatures being a useful tool for checking that collisions are working effectively.*

## 2.4 EVAPORATION

Compare some results to those predicted by the theory of walraven [27] and the other guy [32].

As demonstrated by Wu et al [2, 3] we can use the DSMC method to simulate evaporative cooling. There has been a lot of theoretical investigation into the evolution of cold gases under forced evaporative cooling [31–33], giving us a good basis for analysis. We will use the results of Luiten et al [32] to validate to our simulations. In their work Luiten et al find that the rate of change of total energy due to evaporation is given by

$$\dot{E} = \left( \eta + \frac{W_{\text{ev}}}{V_{\text{ev}}} \right) \dot{N} k_B T,$$

where the effective volume for elastic collisions leading to evaporation,  $V_{\text{ev}}$  is given by

$$V_{\text{ev}} = \frac{\Lambda}{k_B T} \int_0^{\epsilon_t} \rho(\epsilon) \left[ (\epsilon_t - \epsilon - k_B T) e^{-\epsilon/k_B T} + k_B T e^{-\eta} \right] d\epsilon$$

and the volume  $W_{\text{ev}} = V_{\text{ev}} - X_{\text{ev}}$ , with

$$X_{\text{ev}} = \frac{\Lambda}{k_B T} \int_0^{\epsilon_t} \rho(\epsilon) \left[ k_B T e^{-\epsilon/k_B T} - (\epsilon_t - \epsilon + k_B T) e^{-\eta} \right] d\epsilon.$$

If we use the expression for an isotropic power law potential (2.2) from section 2.1 we can find a (rather complicated) expression for this ratio of volumes

$$\frac{X_{\text{ev}}}{V_{\text{ev}}} = \frac{2 \left( 2(2\gamma + 2\eta + 5)\eta^{\gamma + \frac{3}{2}} + e^{\eta} \left( (2\gamma + 3)(2\gamma + 5)\Gamma\left(\gamma + \frac{3}{2}, \eta\right) - 4\Gamma\left(\gamma + \frac{7}{2}\right) \right) \right)}{e^{\eta}(-2\gamma + 2\eta - 5) \left( (2\gamma + 3)(2\gamma + 5)\Gamma\left(\gamma + \frac{3}{2}, \eta\right) - 4\Gamma\left(\gamma + \frac{7}{2}\right) \right) - 2(2\gamma + 5)^2 \eta^{\gamma + \frac{3}{2}}},$$

where  $\Gamma[a, z] = \int_z^{\infty} t^{a-1} e^{-t} dt$  is the incomplete gamma function and  $\Gamma[a] = \int_0^{\infty} t^{a-1} e^{-t} dt$  is the Euler gamma function. It might be immediately obvious from the equation above, but for a given  $\gamma$  this ratio has a maximum of 1 at  $\eta = 0$  and is a monotonically decreasing function of  $\eta$ . I have included this to illustrate a rather unintuitive result. That is that the rate of change of the total energy for an evaporatively cooled gas is not only a function of the evaporation parameter  $\eta$ , but also a function of the trapping parameter  $\gamma$ . Perhaps if we reflect on the thermalisation experiments we have done in the previous sections 2.3.1 and ?? it is not so surprising that this is the case.

If we now differentiate the equation for the total energy of the gas,  $E = (\frac{3}{2} + \gamma) N k_B T$ , with respect to time and combine it with equation (??) we can show

$$\frac{\dot{T}}{T} = \left( \frac{\eta + \frac{W_{\text{ev}}}{V_{\text{ev}}}}{\frac{3}{2} + \gamma} - 1 \right) \frac{\dot{N}}{N}. \quad (2.5)$$

Keeping in mind the maximal value for  $W_{\text{ev}}/V_{\text{ev}}$  is 1 we can see from the above that we require  $\eta > \gamma + 1/2$  for the temperature to decrease as the

number of atoms decreases. Further more we can note the larger  $\eta$  is the more efficient the evaporative cooling will be i.e. a smaller loss of atoms will result in a larger decrease in temperature.

We can also investigate how the density of the gas changes with the number of atoms. Recall in section 2.1 we claimed the density would increase as we removed atoms (how can this be?!). Using the relationship  $N = n_0 V_e$  and the subsequent derivative  $\dot{N} = \dot{n}_0 V_e + n_0 \dot{V}_e$ , and combining this with the results from table 2.1 and equation (2.5) we have

$$\frac{\dot{n}_0}{n_0} = \left( 1 - \gamma \left( \frac{\eta + \frac{W_{ev}}{V_{ev}}}{\frac{3}{2} + \gamma} - 1 \right) \right) \frac{\dot{N}}{N}. \quad (2.6)$$

Thus we see that for the density of the gas to increase as the number of atoms decreases we require that  $\eta > \gamma + 3/2 + 3/2\gamma$ . It is clear from equation (2.6) that the larger  $\gamma$  is the greater increase in density we will have for a given loss of atoms.

Finally we can see how the degeneracy parameter,  $D = n_0 \Lambda^3$ , changes with the loss of atoms

$$\frac{\dot{D}}{D} = \left( \gamma - \eta - \frac{W_{ev}}{V_{ev}} + \frac{5}{2} \right) \frac{\dot{N}}{N}. \quad (2.7)$$

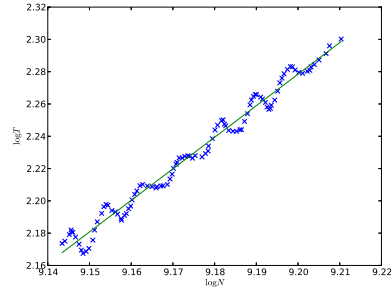
So for  $\eta > \gamma + 3/2$  we will have an increase in the degeneracy parameter as the number of atoms decreases. Here is the definitive result that drives the desire to evaporate in a quadrupole potential. We can see that the larger  $\gamma$  is the greater the increase in the degeneracy parameter will be for a given  $\eta$ . Thus if we can use a quadrupole trap, with  $\gamma = 3$ , we will reach the quantum limit with the minimum atom loss.

## 2.5 DSMC SIMULATIONS OF EVAPORATION

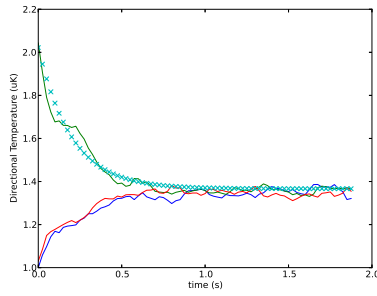
Armed with the relationships from section 2.4 we can investigate the accuracy of the DSMC when applied to the evaporative cooling of cold atoms.

## 2.6 ADIABATICITY

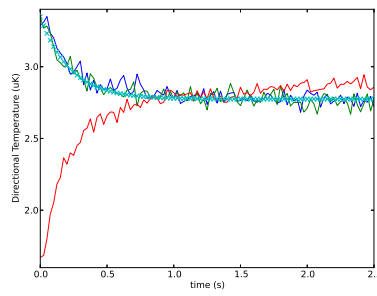
Have a look at squeezing the magnetic trap both diabatically and adiabatically.



(a)  $\eta$  should equal 7, here it is equal to 7.86

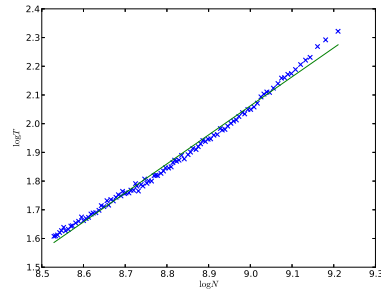


(b) I want this to be a plot of no vs N.

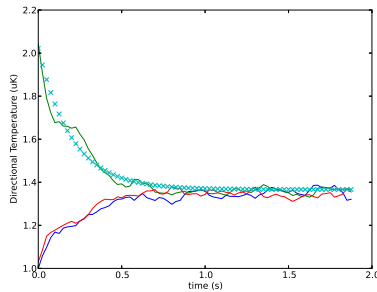


(c) Not sure what plot tp put here

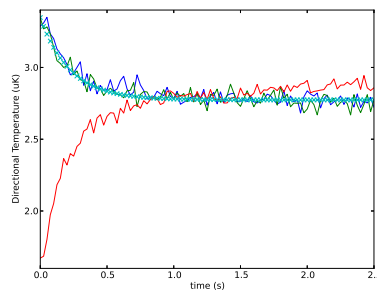
Figure 2.4: IP trap evaporation.



(a)  $\eta$  should equal ?(check the paper), here it is equal to 5



(b) I want this to be a plot of no vs N.



(c) Not sure what plot tp put here

Figure 2.5: Quadrupole trap evaporation.





## MAJORANA INTERLUDE

---

### 3.1 MAJORANA SPIN FLIPS

$$\frac{\partial}{\partial t} \tag{3.1}$$

Talk about Majorana problem, history, derive formula etc

### 3.2 LANDAU ZENER FORMULA

Content

### 3.3 LOSS RATES 'N' STUFF

derive the loss rate formulae used in all the literature.



To include the effects of Majorana spin flips in our DSMC simulations we will obviously have to develop some semiclassical method i. e. simulate the positions of the atoms classically using the DSMC method and simulate the internal state of the atom with a quantum mechanical approach. One such approach would be to use the Ehrenfest theorem [34] to calculate the average force applied to an atom based on its current internal state (I have given a brief pseudo-code in listing 4.1). Using this method we would evolve the internal state of the atom using the Schrödinger equation then, using the internal state of the atom, we can calculate the expectation value of the force to use in evolving the position of the atom.

Unfortunately this technique is not a viable solution, as we will demonstrate in this chapter. While we are able to capture some of the interesting physics (usually short term) of the Majorana spin flip using the Ehrenfest approach, it just fails over long simulation periods.

#### 4.1 SIMULATING SCHRÖDINGER EQUATION

To make use of the proposed Ehrenfest method (EM) we need to be able to accurately solve the Schrödinger equation. Some of the more straightforward approaches might be to apply a finite difference technique directly to the pde, however these methods are not generally conservative [? ]. In fact the techniques that are considered more stable generally have some non-physical numerical dissipation as a result of the approximations made [? ] (or even show?).

The approach we have employed here, and in chapter 5, is to make use of the unitary time evolution operator [? ]. The main benefit of this approach is, as the name suggests, the operator is unitary and hence inherently conserves probability. The unitary time evolution operator is defined as follows

$$\hat{U}(t_0, t_0 + \Delta t) = \exp \left[ -\frac{i}{\hbar} \int_{t_0}^{t_0 + \Delta t} \hat{H}(t) dt \right]. \quad (4.1)$$

That is for a time dependent Hamiltonian we can evolve the state of our wavefunction,  $|\psi\rangle$ , through a moment of time  $\Delta t$ , through the application of the time evolution operator,  $\hat{U}$ ,

$$|\psi(t_0 + \Delta t)\rangle = \hat{U}(t_0, t_0 + \Delta t) |\psi(t_0)\rangle.$$

This method is especially useful for our two level system as we can explicitly derive an expression for the  $2 \times 2$  matrix form of  $\hat{U}$ . Recall from

section 1.1 that the Hamiltonian for a magnetic moment in a magnetic field is given by

$$\hat{H} = -\hat{\boldsymbol{\mu}} \cdot \mathbf{B},$$

which can be expressed in matrix form as

$$\hat{H} = \frac{1}{2}g_s\mu_B \begin{bmatrix} B_z & B_x - \imath B_y \\ B_x + \imath B_y & -B_z \end{bmatrix}.$$

In general the magnetic field components are functions of position, which, for the atoms is a function of time. For a general magnetic field we do not know explicitly what the time dependance will be and so we will not be able to explicitly integrate the Hamiltonian as required by equation (4.1). So we will have to make the assumption that our time steps are very small,  $\Delta t \ll 1$ , so that over the time step the Hamiltonian remains relatively constant. In this limit we have,  $\int \hat{H} dt = \hat{H}\Delta t$ , so that the time evolution operator becomes

$$\hat{U}(t_0, t_0 + \Delta t) = \exp \left[ -\imath \frac{g_s\mu_B\Delta t}{2\hbar} \begin{bmatrix} B_z & B_x - \imath B_y \\ B_x + \imath B_y & -B_z \end{bmatrix} \right], \quad (4.2)$$

$$= \begin{bmatrix} \cos \theta - \imath n_z \sin \theta & -(n_y + \imath n_x) \sin \theta \\ (n_y - \imath n_x) \sin \theta & \cos \theta + \imath n_z \sin \theta \end{bmatrix}, \quad (4.3)$$

where  $\theta = g_s\mu_B\Delta t|\mathbf{B}|/2\hbar$  and  $n_k = B_k/|\mathbf{B}|$  are the directional components of the magnetic field normal vector. This simple closed form expression makes it very easy to implement the unitary evolution operator method numerically.

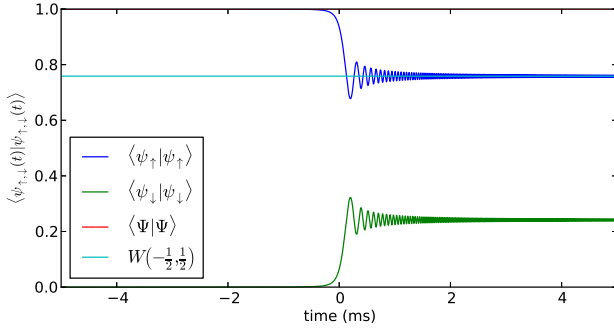
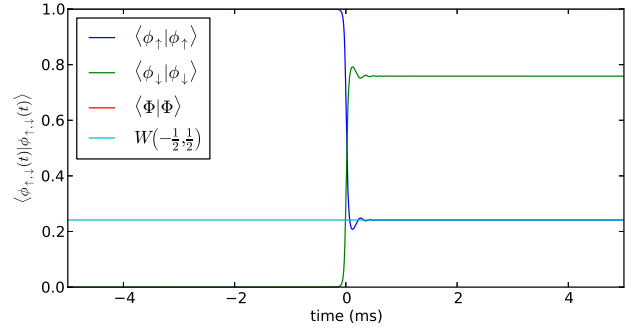
## 4.2 SCHRÖDINGER SIMULATIONS

To test out this technique lets just numerically solve the original Majorana problem (3.1). In figure 4.1 I have simulated two scenarios: a spin flip (figs 4.1a, 4.1b) and a not flip (figs 4.1c, 4.1d). Each scenario is plotted in two seperate reference frames: the laboratory frame and the co-rotating frame. The laboratory frame is the frame in which the spin up direction is aligned with the z-axis, the co-rotating frame is the frame in which the spin up direction is aligned with the magnetic field. The laboratory frame is the frame in which the differential equation is set, however in this frame it can become a little confusing about whether a particular spin state is flipped or not. In both of the simulations the direction of the magnetic field changes at  $t = 0$ , so the orientation of the spin up direction in the lab frame also changes. In the co-rotating frame it is always clear which state is the spin up state.

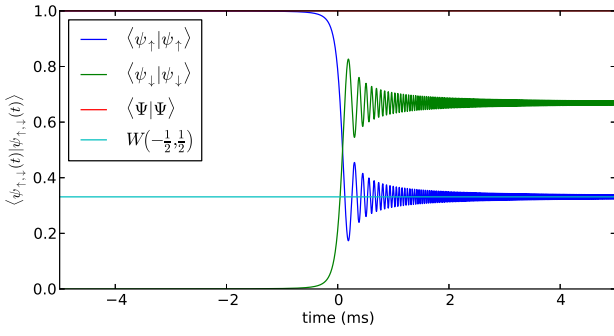
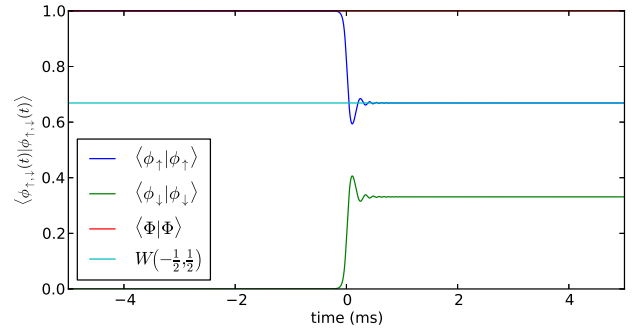
Figures 4.1a and 4.1b both illustrate a Majorana spin flip. In this simulation we used the magnetic field  $\mathbf{B} = (0.1, 0.0, 2500t) \text{ mT}$ , and began at  $t = -15 \text{ ms}$  where the population in the spin component in the lab frame

*Make a side note about higher order integration.*

*We find the spin up and spin down components in the co-rotating frame by projecting onto the "local" magnetic field. We do this using the projection operator,  $|\Phi_{\uparrow,\downarrow}\rangle = \hat{P}_{\uparrow,\downarrow}|\Psi\rangle$ , where the projection operator is given by  $\hat{P} = ??$ .*

(a) Lab frame flip,  $B_t = 1 \times 10^{-7}$ 

(b) Rotating frame flip

(c) Lab frame no flip,  $B_t = 2 \times 10^{-7}$ 

(d) Rotating frame no flip

Figure 4.1: Simulating the no majorana spin flip

Listing 4.1: Psuedo-code algorithm for a single Ehrenfest method time step

1	Calculate force using current spin state: $\mathbf{F}_n = \langle \Psi_n   \hat{\mathbf{F}}_n   \Psi_n \rangle$ .
2	Evolve wavefunction using time evolution operator: $ \Psi_{n+1}\rangle = \hat{U}_n  \Psi_n\rangle$ .
3	Evolve velocity using the average force: $\mathbf{v}_{n+1} = \mathbf{v}_n + \mathbf{F}_n \Delta t / m$ .
4	Evolve position using the new velocity: $\mathbf{x}_{n+1} = \mathbf{x}_n + \mathbf{v}_{n+1} \Delta t$ .

is less than  $10^6$  (although we have plotted a smaller time window in figure 4.1). We can see the distinct difference between the behaviour of the spin populations in the two different reference frames. The initial wavefunction was chosen such that the population of the spin up component in the lab frame was 1. Figure 4.1b clearly displays a change in the most probable state, whereas in figure 4.1a it is not so clear. Again this is because in the lab frame the spin up direction changes at  $t = 0$  when the sign of the  $z$  component of the magnetic field moves from negative to positive. Figures 4.1c and 4.1d results from a simulation with  $\mathbf{B} = (0.2, 0.0, 2500t)$  mT. In these plots we see the converse behaviour in the state populations, indicating that no spin flip has occurred.

For both simulations we have used a time step of  $\Delta t = 1 \mu\text{s}$ . This may seem overkill given the rate of change of the magnetic field can be characterised by  $\tau_B = |\mathbf{B}| / |\partial_t \mathbf{B}| = 15 \text{ ms}$  at the beginning of the simulation. However there is another time scale that must be considered in a simulation like this, that is the period of a Larmor precession,  $T_L = 2\pi\hbar / g_s \mu_B |\mathbf{B}| = 3.81 \mu\text{s}$  at the beginning of the simulation. While we do not expect the spin to precess for the first half of the simulation when it is completely aligned with the magnetic field, it is the period close to the field minimum and beyond that will experience Larmor precession. In fact the wiggles after the spin flip occur at the Larmor precession frequency. For example, look at one period of oscillation around  $t = 0.3 \text{ ms}$ , here the Larmor precession period will be,  $T_L = 0.19 \text{ ms}$ , exactly as simulated (\*\*MAKE INSET IN FIGURE TO SHOW LARMOR PRECESSION RATE\*\*).

*The astute reader may be confused by line 4 of the pseudo-code in listing 4.1.*

*The appearance of the  $n + 1^{\text{th}}$  velocity when calculating the  $n + 1^{\text{th}}$  position is not how one might implement the standard Euler integration method. Here we have used an implementation of the Symplectic Euler method [?], which has better energy conserving properties than the standard forward Euler. This technique still has the same order accuracy with time, and introduces no added computational complexity, yet we gain some extra stability in the total energy of the atom.*

### 4.3 SINGLE ATOM SPIN FLIPS

Confident in our ability to accurately simulate the Schrödinger equation, in our regime of interest, we may begin to apply the Ehrenfest method to simulating spin flips of real atoms. The first step is to first see whether or not we can simulate the spin flip of a single atom. I have given a pseudo-code example for a single time step of the Ehrenfest algorithm in listing 4.1<sup>1</sup>.

Figure 4.2 shows the results from one such simulation. This simulation was of a rubidium 87 atom that began at  $z = -5 \mu\text{m}$  with a zero initial velocity. Again the initial wavefunction was chosen so that it would be

<sup>1</sup> Note in listing 4.1 that we have denoted the discrete approximation to a continuous variable as,  $g_n \approx g(t_n)$ .

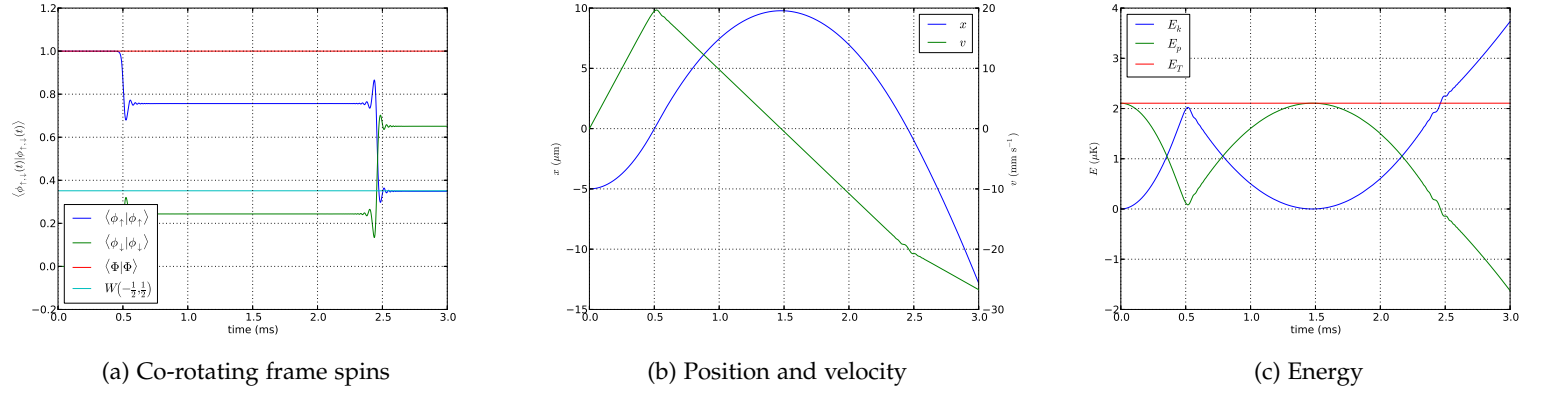


Figure 4.2: No flip and flip in the same simulation.

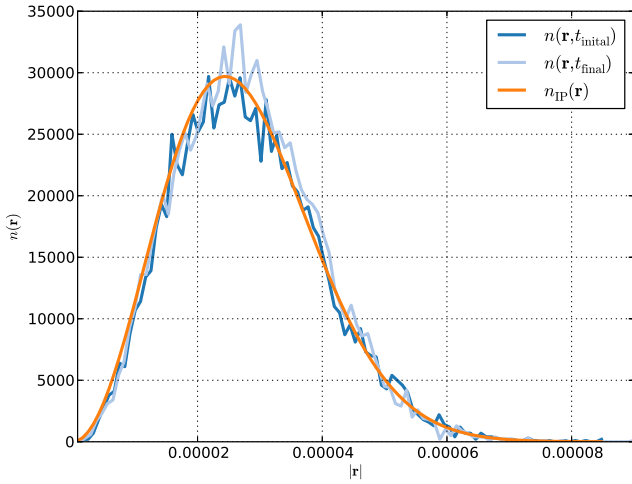
completely spin up in the co-rotating frame. The magnetic field was given by  $\mathbf{B} = (B_x, 0, B'_z z)$ , with  $B_x = 1 \mu\text{T}$  and  $B'_z = 2.5 \text{ Tm}^{-1}$ <sup>2</sup>. This is a fabulous example of how well the Ehrenfest method can work. Figure 4.2a displays how well the spin populations are simulated. Again they agree with the predictions of the Majorana formula and the total probability is conserved. In figure 4.2b I have plotted the position and velocity of the atom as it moves through time. We can see how the atom remains trapped after the first partial flip and is then completely ejected from the trapped once it has flipped. Finally figure 4.2c shows how the total energy of the atom is conserved throughout the simulation (even after it has flipped). So things seem to be working quite well, but earlier I alluded to the fact that the Ehrenfest method is not suitable to this kind of problem, so what is wrong? I will let you stew on this for a few sections while we investigate the behaviour of a full gas simulation.

Say how I can still use the Majorana formula here.  
 $c = v(t=0)B'_z$ .

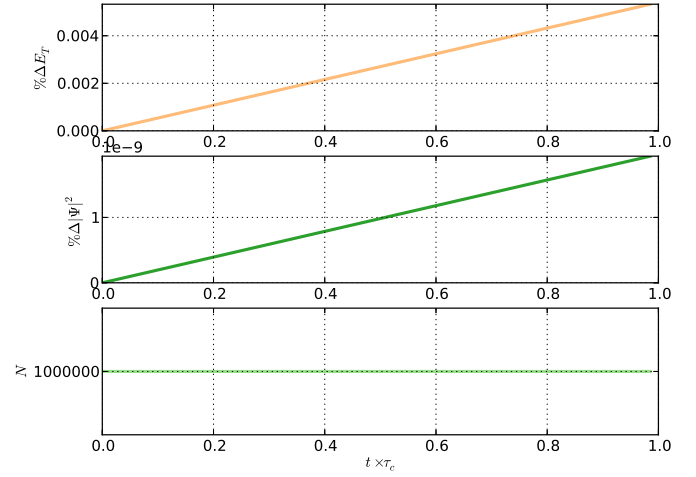
#### 4.4 FULL GAS SIMULATIONS

Convinced that our Ehrenfest method can simulate spin flips and conserves both energy and probability we can begin to run some full gas simulations. Majorana spin flips only occur when there is a sharp transition in magnetic field direction, like that transition that is present around the centre of a quadrupole trap. An IP trap does not have this kind of transition, thus we would expect a very small number (o) of spin flips to occur as a result of the IP field configuration. As a cautionary test we will simulate a gas trapped in an IP trap using the Ehrenfest method.

<sup>2</sup> I am aware that this magnetic field does not satisfy Maxwell's equations, but it serves as a nice example and more closely aligns with the field considered by Majorana.



(a) IP Distribution



(b) IP Conservation

Figure 4.3: Ehrenfest method for a gas in an IP trap.

#### 4.4.1 Ioffe Pritchard Trap

The IP trap will remove any of the complex dynamics (and atom loss) we would experience from Majorana loss. This will allow us to simulate the energy and probability conserving characteristics of the method, as well as ensure that the simulated particle dynamics are as expected.

The results from a simulation of  $10^6$  rubidium 87 atoms at  $2 \mu\text{K}$  in an IP with  $B_0 = 0.01 \text{ T}$ ,  $B' = 20.0 \text{ Tm}^{-1}$  and  $B'' = 40,000 \text{ Tm}^{-2}$  over a period of approximately 10 collision times ( $10\tau_c$ ) are shown in figure 4.3. In this figure I have tried to show the conservative properties of the Ehrenfest method. Figure 4.3a illustrates the radial distribution of particles. I have drawn the distribution at the beginning and the end of the simulation, as well as contrast it with the analytic result for a thermal gas. As we can see the numerical result is very stable and agrees well with the analytic prediction. In figure 4.3b I have illustrated the change in the quantities we would expect to be conserved in a simulation like this. The top graph shows the percentage change in the average total energy, the middle graph shows the percentage change in the average norm of the wavefunction and the bottom graph shows the number of atoms.

First of all we can note there is no change in the number of atoms i.e. no Majorana spin flips. This simulation has the same evaporation code running as we developed in section 2.4, with the evaporation condition that if  $P_z < 0$  the atom is removed. This is due to the presence of the non-zero field bias,  $B_0$ , which ensures that the Larmor precession rate is always greater than the rate of change of the magnetic field direction. Second we can see a linear increase in the total energy and wavefunction norm. How can this be, I thought we were using fancy symplectic methods that were

The density distribution for a thermal gas is  $n(\mathbf{r}) = n_0 \exp[-\mathcal{U}(\mathbf{r})/k_B T]$ .



designed to conserve these quantities. I have two responses to that question, the first is can we really call a %0.005 (that is 1 in 20,000) increase a significant change? For the simulation I have run here this corresponds to the total energy changing by 0.3 nK, not we might consider a significant increase in temperature. However, we can argue that there is a clear linear trend and if we anticipate running extended simulations this might be something that we wish to keep in mind. Although I wouldn't consider this deal breaker. My second response would be that the time step I have used is far too large. For this simulation I have used the time step,  $\Delta t = 5$  ns. This might seem quite small but compared to the Larmor period at the the average radius,  $T_L \approx 10^{-8}$  s, it isn't that great. Not only does this mean on average we are only sampling the wavefunction twice per Larmor rotation, but out on the edges of the gas we are doing far worse! Of course we could reduce the time step, and this would improve our energy conservation, but to be able to run these simulations in a reasonable time frame we must accept a certain level of non-conservation in our total energy and wavefunction norm.

Overall this seems to have worked quite well and yet I keep saying that the Ehrenfest method is not suitable for our simulations. Let's now try to run a simulation in a quadrupole trap and see how effective the method is.

#### 4.4.2 *Quadrupole Trap*

Content



I guess I need to talk about the MCWF method here, this could be difficult.

### 5.1 SINGLE ATOM SPIN FLIPS

Just like we did with the Ehrenfest method in section 4.3 we can begin by simulating the a spin flip of a single atom in a Majorana type trap. To make the comparison between the two methods fair we will again use the same magnetic field,  $\mathbf{B} = (B_x, 0, B'_z z)$ , with  $B_x = 1 \mu\text{T}$  and  $B'_z = 2.5 \text{ Tm}^{-1}$ . Our rubidium 87 atom will also have the same initial conditions,  $z = -5 \mu\text{m}$  and zero initial velocity,  $v_z = 0 \text{ ms}^{-1}$ . Finally we will use the same simulation time step,  $\Delta t = 0.1 \mu\text{s}$ . The only difference here is that we must average the result over a large number of simulations, in this case we have run  $10^5$  independent simulations.

At last, in figure 5.1 we have some convincing proof of the failure of the Ehrenfest method. First let's get the boring stuff out of the way. Figure 5.1a illustrates that the MCWF method conserves probability, similarly figure 5.1c shows the energy conservation of the method. Now let's compare the differences between the Ehrenfest and MCWF methods. We'll start by comparing the wavefunction evolution depicted in figure 5.1a. Here we see the two methods agree perfectly for the first magnetic field minimum crossing. However, at around 1.5 ms we see the MCWF method make, what looks to be another spin flip, and then another at 2.5 ms. How can this be? What is it that causes the particles in the MCWF method to experience an extra spin flip? This questions is most clearly illustrated in figure 5.1b. The bold lines indicate the averaged trajectories of the MCWF particles. Again up

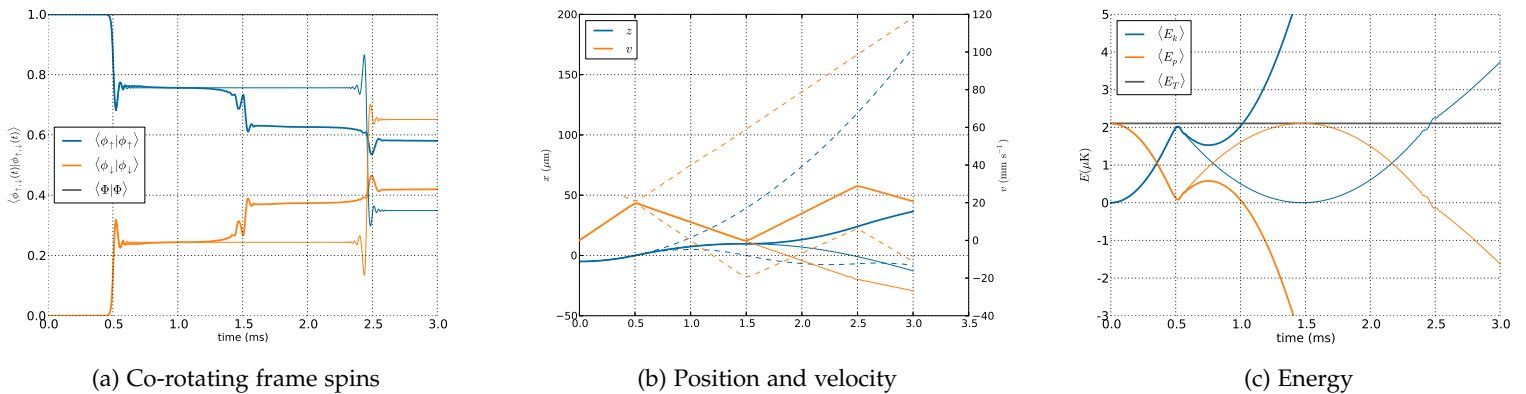


Figure 5.1: No flip and flip in the same simulation mcwf.

until the 1.5 ms mark the two approaches (Ehrenfest and MCWF) agree exactly. So what is it that happens at 1.5 ms that causes this deviation? Consider the trajectories shown by the dashed lines. These lines represent the average trajectories of all the particles who are considered to be in a trapped state. Conversely the dash-dotted lines are the untapped state. While the average of these two trajectories produces the same result as the Ehrenfest method (as we might expect), the physical path taken by the particles is completely different. So the reason for the apparent extra spin flip at 1.5 ms is due to the extra crossing of the field minimum experienced by the particles that remain in the trapped state. So what happens in the Ehrenfest simulation? What is it that produces its failure? The Ehrenfest method will move particle along the trajectory described by the average force. At 0.5 ms after the first crossing of the field minimum the particle experiences a partial flip. Since the particle is moved with the average force the trapping force of the particle is now weaker and it is effectively trapped in a looser magnetic field. While on average this may be a reasonable way to think about the problem, we have already seen that it does not produce the correct dynamics for particles moving in a simple one-dimensional trap.

How does this result explain the disagreement of the Ehrenfest method with the test done in section 4.4.2? When a particle experiences a partial flip the Ehrenfest method will then subject it to a weaker trapping force, essentially loosening or widening the trapping potential. So in figure ?? as the particles of the gas slowly begin to tip over, from the cumulative effect of many partial flips, the gas begins to unnaturally widen. As a result the calculated temperature is higher than what one would physically expect. In practice we know that an atom is either in a trapped state or an untrapped state (not partially in both). So a real trapped gas that is subjected to Majorana spin flips should not display a widening due to the weakening trapping potential, it should only exhibit atom loss due to the fully flipped atoms leaving the trap<sup>1</sup>.

So why does the Ehrenfest method seem to work for the Ioffe Pritchard trap? We do not expect atoms in the IP trap to undergo any kind of spin flip. The geometry of the trap is such that the rate of change of the magnetic field direction is always (JUSTIFY?) less than the Larmor precession rate. So the particles in the simulation shown in figure 4.3 are always subjected to the full trapping potential.

## 5.2 FULL GAS SIMULATIONS

### Content

<sup>1</sup> Of course this will also result in a widening of the trap due to the heating effect cause by the selective removal of the least energetic particles.

5.2.1 *Ioffe Pritchard Trap*

Content

5.2.2 *Quadrupole Trap*

Content



## Part III

### FEMDVR

You can put some informational part preamble text here. Illo principalmente su nos. Non message occidental angloromanic da. Debitas effortio simplicate sia se, auxiliar summarios da que, se avantiate publicationes via. Pan in terra summarios, capital interlingua se que. Al via multo esser specimen, campo responder que da. Le usate medical addresses pro, europa origine sanctificate nos se.





## FEMDVR

---

### 6.1 1D FEMDVR

Content

#### 6.1.1 *Scaling Comparison to CPU*

Content

#### 6.1.2 *Real Simulation*

Content

### 6.2 3D FEMDVR

Content

#### 6.2.1 *Knots*

Content



## Part IV

### CUDA

You can put some informational part preamble text here. Illo principalmente su nos. Non message occidental angloromanic da. Debitas effortio simplicate sia se, auxiliar summarios da que, se avantiate publicationes via. Pan in terra summarios, capital interlingua se que. Al via multo esser specimen, campo responder que da. Le usate medical addresses pro, europa origine sanctificate nos se.



## CUDA DSMC

---

### 7.1 CUDA

Content

#### 7.1.1 *Parallelisation*

Content

### 7.2 SPEED UP

Content

#### 7.2.1 *Some simulations*

Content



## Part V

### APPENDIX





## THERMAL PHYSICS

---

### A.1 COLLISION RATES IN THERMAL GASES

### A.2 THERMALISATION

#### A.2.1 *Walraven Thermalisation*







## MOTION INTEGRATION

---

In this appendix we will explain in detail the different methods of integrating the Newtonian motion of particles and specifically how we have gone about it.

### C.1 EULER METHOD

$$x_{n+1} = x_n + v_n \Delta t, \quad (\text{C.1})$$

$$v_{n+1} = v_n + a_n \Delta t. \quad (\text{C.2})$$

### C.2 SEMI-IMPLICIT EULER METHOD

$$x_{n+1} = x_n + v_n \Delta t, \quad (\text{C.3})$$

$$v_{n+1} = v_n + a_{n+1} \Delta t. \quad (\text{C.4})$$

### C.3 VERLET ALGORITHM

Sometimes referred to as the Störmer-Verlet method (see wikipedia page it's pretty good), it was made popular by Verlet in 1976 [35]. The Verlet algorithm can be derived from the Taylor series expansions for position as follows,

$$\mathbf{r}(t_{n+1}) = \mathbf{r}(t_n) + k\mathbf{v}(t_n) + \frac{1}{2}k^2\mathbf{a}(t_n) + \mathcal{O}(k^3), \quad (\text{C.5a})$$

$$\mathbf{r}(t_{n-1}) = \mathbf{r}(t_n) - k\mathbf{v}(t_n) + \frac{1}{2}k^2\mathbf{a}(t_n) + \mathcal{O}(k^3), \quad (\text{C.5b})$$

we can now add equations (C.5a) and (C.5b) together to get

$$\begin{aligned} \mathbf{r}(t_{n+1}) + \mathbf{r}(t_{n-1}) &= 2\mathbf{r}(t_n) + k^2\mathbf{a}(t_n) + \mathcal{O}(k^4), \\ \Rightarrow \mathbf{r}(t_{n+1}) &= 2\mathbf{r}(t_n) - \mathbf{r}(t_{n-1}) + k^2\mathbf{a}(t_n) + \mathcal{O}(k^4),. \end{aligned} \quad (\text{C.6})$$

We can see from equation (C.6) that the leap frog method is fourth order in time. However, we can also note that the velocities do not explicitly appear in the method, this means we need to derive them from positions. A simple approximation would be to use the midpoint method

$$\mathbf{v}(t_n) = \frac{1}{2}k(\mathbf{r}(t_{n+1}) - \mathbf{r}(t_{n-1})) \quad (\text{C.7})$$

## C.4 LEAP FROG METHOD

[36]

$$x_n = x_{n-1} + v_{i-1/2} \Delta t, \quad (\text{C.8})$$

$$v_{n+1/2} = v_{n-1/2} + a_n \Delta t. \quad (\text{C.9})$$

## C.5 VELOCITY VERLET

[37]

$$x_{n+1} = x_n + v_i \Delta t + \frac{1}{2} a_n \Delta t^2, \quad (\text{C.10})$$

$$v_{n+1} = v_n + \frac{1}{2} (a_n + a_{n+1}) \Delta t. \quad (\text{C.11})$$

## C.6 BEEMAN'S ALGORITHM

[38]

$$x_{n+1} = x_n + v_n \Delta t + \frac{1}{6} (4a_n - a_{n-1}) \Delta t^2, \quad (\text{C.12})$$

$$v_{n+1} = v_n + \frac{1}{6} (2a_{n+1} + 5a_n - a_{n-1}) \Delta t. \quad (\text{C.13})$$

## DIRECT SIMULATION MONTE CARLO

Aliquam lectus. Vivamus leo. Quisque ornare tellus ullamcorper nulla. Mauris porttitor pharetra tortor. Sed fringilla justo sed mauris. Mauris tellus. Sed non leo. Nullam elementum, magna in cursus sodales, augue est scelerisque sapien, venenatis congue nulla arcu et pede. Ut suscipit enim vel sapien. Donec congue. Maecenas urna mi, suscipit in, placerat ut, vestibulum ut, massa. Fusce ultrices nulla et nisl.

Etiam ac leo a risus tristique nonummy. Donec dignissim tincidunt nulla. Vestibulum rhoncus molestie odio. Sed lobortis, justo et pretium lobortis, mauris turpis condimentum augue, nec ultricies nibh arcu pretium enim. Nunc purus neque, placerat id, imperdiet sed, pellentesque nec, nisl. Vestibulum imperdiet neque non sem accumsan laoreet. In hac habitasse platea dictumst. Etiam condimentum facilisis libero. Suspendisse in elit quis nisl aliquam dapibus. Pellentesque auctor sapien. Sed egestas sapien nec lectus. Pellentesque vel dui vel neque bibendum viverra. Aliquam porttitor nisl nec pede. Proin mattis libero vel turpis. Donec rutrum mauris et libero. Proin euismod porta felis. Nam lobortis, metus quis elementum commodo, nunc lectus elementum mauris, eget vulputate ligula tellus eu neque. Vivamus eu dolor.

## D.1 APPENDIX SECTION TEST

Nulla in ipsum. Praesent eros nulla, congue vitae, euismod ut, commodo a, wisi. Pellentesque habitant morbi tristique senectus et netus et malesuada fames ac turpis egestas. Aenean nonummy magna non leo. Sed felis erat, ullamcorper in, dictum non, ultricies ut, lectus. Proin vel arcu a odio lobortis euismod. Vestibulum ante ipsum primis in faucibus orci luctus et ultrices posuere cubilia Curae; Proin ut est. Aliquam odio. Pellentesque massa turpis, cursus eu, euismod nec, tempor congue, nulla. Duis viverra gravida mauris. Cras tincidunt. Curabitur eros ligula, varius ut, pulvinar in, cursus faucibus, augue.

*More dummy text*

Nulla mattis luctus nulla. Duis commodo velit at leo. Aliquam vulputate magna et leo. Nam vestibulum ullamcorper leo. Vestibulum condimentum rutrum mauris. Donec id mauris. Morbi molestie justo et pede. Vivamus eget turpis sed nisl cursus tempor. Curabitur mollis sapien condimentum nunc. In wisi nisl, malesuada at, dignissim sit amet, lobortis in, odio. Aenean consequat arcu a ante. Pellentesque porta elit sit amet orci. Etiam at turpis nec elit ultricies imperdiet. Nulla facilisi. In hac habitasse platea dictumst. Suspendisse viverra aliquam risus. Nullam pede justo, molestie nonummy, scelerisque eu, facilisis vel, arcu.

LABITUR BONORUM PRI NO	QUE VISTA	HUMAN
fastidii ea ius	germano	demonstratea
suscipit instructor	titulo	personas
quaestio philosophia	facto	demonstrated

Table D.1: Autem usu id.

Listing D.1: A floating example

```

1 for i:=maxint to 0 do
  begin
    { do nothing }
  end;

```

## D.2 ANOTHER APPENDIX SECTION TEST

Curabitur tellus magna, porttitor a, commodo a, commodo in, tortor. Donec interdum. Praesent scelerisque. Maecenas posuere sodales odio. Vivamus metus lacus, varius quis, imperdiet quis, rhoncus a, turpis. Etiam ligula arcu, elementum a, venenatis quis, sollicitudin sed, metus. Donec nunc pede, tincidunt in, venenatis vitae, faucibus vel, nibh. Pellentesque wisi. Nullam malesuada. Morbi ut tellus ut pede tincidunt porta. Lorem ipsum dolor sit amet, consectetur adipiscing elit. Etiam congue neque id dolor.

Donec et nisl at wisi luctus bibendum. Nam interdum tellus ac libero. Sed sem justo, laoreet vitae, fringilla at, adipiscing ut, nibh. Maecenas non sem quis tortor eleifend fermentum. Etiam id tortor ac mauris porta vulputate. Integer porta neque vitae massa. Maecenas tempus libero a libero posuere dictum. Vestibulum ante ipsum primis in faucibus orci luctus et ultrices posuere cubilia Curae; Aenean quis mauris sed elit commodo placerat. Class aptent taciti sociosqu ad litora torquent per conubia nostra, per inceptos hymenaeos. Vivamus rhoncus tincidunt libero. Etiam elementum pretium justo. Vivamus est. Morbi a tellus eget pede tristique commodo. Nulla nisl. Vestibulum sed nisl eu sapien cursus rutrum.



## NON-DIMENSIONALISATION

---

### E.1 QUASI - 1D GPE

Let's just start with writing out the full quasi-one-dimensional three component equation in a harmonic potential

$$\begin{aligned} i\hbar \frac{\partial}{\partial t} f_+ = & \left( -\frac{\hbar^2}{2m} \frac{\partial^2}{\partial z^2} + \frac{1}{2} m \omega_z^2 z^2 + E_+ + E_\perp + c_0 N \eta \rho \right. \\ & \left. + c_2 N \eta (\rho_+ + \rho_0 - \rho_-) \right) f_+ + c_2 N \eta f_0^2 f_-^*, \end{aligned} \quad (\text{E.1a})$$

$$\begin{aligned} i\hbar \frac{\partial}{\partial t} f_0 = & \left( -\frac{\hbar^2}{2m} \frac{\partial^2}{\partial z^2} + \frac{1}{2} m \omega_z^2 z^2 + E_0 + E_\perp + c_0 N \eta \rho \right. \\ & \left. + c_2 N \eta (\rho_+ + \rho_-) \right) f_0 + 2c_2 N \eta f_+ f_- f_0^*, \end{aligned} \quad (\text{E.1b})$$

$$\begin{aligned} i\hbar \frac{\partial}{\partial t} f_- = & \left( -\frac{\hbar^2}{2m} \frac{\partial^2}{\partial z^2} + \frac{1}{2} m \omega_z^2 z^2 + E_- + E_\perp + c_0 N \eta \rho \right. \\ & \left. + c_2 N \eta (\rho_- + \rho_0 - \rho_+) \right) f_- + c_2 N \eta f_0^2 f_+^*, \end{aligned} \quad (\text{E.1c})$$

$$\rho \frac{\partial E_\perp}{\partial \chi} + \left( \frac{c_0 N}{2} \rho^2 + \frac{c_2 N}{2} S_2 \right) \frac{\partial \eta}{\partial \chi} = 0. \quad (\text{E.1d})$$

If we make the Thomas Fermi ansatz then the transverse mode energy and the scaling factor are given by

$$E_\perp = \frac{\hbar \omega_\perp}{6} \frac{\chi^2}{a_\perp^2}, \quad (\text{E.2})$$

$$\eta = \frac{4}{3\pi \chi^2}, \quad (\text{E.3})$$

where  $a_\perp = \sqrt{\hbar/m\omega_\perp}$ . If we substitute (E.2) and (E.3) into (E.1d) then we find

$$\chi = \left( \frac{4c_0 N \rho^2 + c_2 N S_2}{m\pi \rho \omega_\perp^2} \right)^{\frac{1}{4}}. \quad (\text{E.4})$$

Now substituting (E.4) back into (E.2) and (E.3) and simplifying we have

$$E_\perp = \sqrt{\frac{m N \omega_\perp^2 (c_0 \rho^2 + c_2 S_2)}{9\pi \rho}}, \quad (\text{E.5})$$

$$\eta = \frac{2}{3} \sqrt{\frac{m \rho \omega_\perp^2}{\pi N (c_0 \rho^2 + c_2 S_2)}}. \quad (\text{E.6})$$

Now we can begin to non-dimensionalise the equations. Let us only consider the non-dimensionalisation of the positive component since the procedure will be exactly the same for all components. We begin by making the substitutions

$$\begin{aligned} t &\rightarrow t_c \tau, \\ z &\rightarrow z_c \zeta, \\ f_+ &\rightarrow f_c u_+. \end{aligned}$$

Equation (E.1a) now becomes

$$\begin{aligned} i\hbar \frac{f_c}{t_c} \frac{\partial}{\partial \tau} u_+ &= \left( -\frac{\hbar^2}{2mz_c^2} \frac{\partial^2}{\partial \zeta^2} + \frac{1}{2} m\omega_z^2 z_c^2 \zeta^2 + f_c E_+ + f_c E_\perp + c_0 f_c N\eta\rho \right. \\ &\quad \left. + c_2 f_c N\eta (\rho_+ + \rho_0 - \rho_-) \right) f_c u_+ + c_2 f_c^2 N\eta u_0^2 u_-^*, \\ i \frac{mz_c^2}{\hbar t_c} \frac{\partial}{\partial \tau} u_+ &= \left( -\frac{1}{2} \frac{\partial^2}{\partial \zeta^2} + \frac{1}{2} \frac{m^2 \omega_z^2 z_c^4}{\hbar^2} \zeta^2 + \frac{mz_c^2}{\hbar^2} f_c [E_+ + E_\perp + c_0 N\eta\rho \right. \\ &\quad \left. + c_2 N\eta (\rho_+ + \rho_0 - \rho_-)] \right) u_+ + \frac{mz_c^2}{\hbar^2} c_2 f_c N\eta u_0^2 u_-^*. \end{aligned}$$

Looking at the coefficient of the  $\zeta^2$  term we can see that if we set it to  $1/2$  we will be able to solve for  $z_c$ ,

$$\begin{aligned} 1 &= \frac{m^2 \omega_z^2 z_c^4}{\hbar^2}, \\ \Rightarrow z_c &= \sqrt{\frac{\hbar}{m\omega_z}}, \end{aligned} \tag{E.7}$$

which is the harmonic oscillator length along the  $z$  axis, a natural length scale for the  $z$  dimension. Now we can turn our attention to the coefficient of the time derivative, and set it to  $i$ ,

$$\begin{aligned} 1 &= \frac{mz_c^2}{\hbar t_c}, \\ &= \frac{m\hbar}{m\hbar\omega_z t_c}, \\ \Rightarrow t_c &= \frac{1}{\omega_z}, \end{aligned} \tag{E.8}$$

which is the angular period of the oscillator, again a natural length scale. Finally we can consider the energy terms. With these we need to choose  $f_c$  such that the dimension of the energy term is one. To cut a long story short, this makes a suitable choice for  $f_c$  to be  $1/\sqrt{z_c}$ . Giving us the final form of the non-dimensionalised equation

$$\begin{aligned} i \frac{\partial}{\partial \tau} u_+ &= \left( -\frac{1}{2} \frac{\partial^2}{\partial \zeta^2} + \frac{1}{2} \zeta^2 + \frac{m}{\hbar^2} \left( \frac{\hbar}{m\omega_z} \right)^{\frac{3}{4}} [E_+ + E_\perp + c_0 N\eta\rho \right. \\ &\quad \left. + c_2 N\eta (\rho_+ + \rho_0 - \rho_-)] \right) u_+ + \frac{m}{\hbar^2} \left( \frac{\hbar}{m\omega_z} \right)^{\frac{3}{4}} c_2 N\eta u_0^2 u_-^*. \end{aligned} \tag{E.9}$$

## E.2 MAJORANA PROBLEM SPIN HALF

The potential energy operator [?] for a magnetic dipole in a field is given by

$$\hat{V} = -\hat{\boldsymbol{\mu}} \cdot \mathbf{B}, \quad (\text{E.10})$$

where  $\hat{\boldsymbol{\mu}}$  is the magnetic dipole operator and  $\mathbf{B}$  is the magnetic field. Which for a spin half particle is

$$\hat{V} = \frac{1}{2} \mu_B g_s \begin{bmatrix} B_z & B_x - iB_y \\ B_x + iB_y & -B_z \end{bmatrix},$$

where  $\mu_B$  is the Bohr magneton [?] and  $g_s$  is the Landé g-factor of the spin- $\frac{1}{2}$  particle. Now we can write the time dependant Schrödinger equation for our system (need to introduce kinetic energy operator as well)

$$i\hbar \partial_t \psi_{\uparrow} = -\frac{\hbar^2}{2m} \partial_{zz} \psi_{\uparrow} + \frac{1}{2} \mu_B g_s B_z \psi_{\uparrow} + \frac{1}{2} \mu_B g_s (B_x - iB_y) \psi_{\downarrow}, \quad (\text{E.11})$$

$$i\hbar \partial_t \psi_{\downarrow} = -\frac{\hbar^2}{2m} \partial_{zz} \psi_{\downarrow} - \frac{1}{2} \mu_B g_s B_z \psi_{\downarrow} + \frac{1}{2} \mu_B g_s (B_x + iB_y) \psi_{\uparrow}. \quad (\text{E.12})$$

Maybe before we non-dimensionalise we will insert or actual values for the magnetic field,  $\mathbf{B} = (B_x, 0, -dB_z z)$ . Now to non-dimensionalise. We make the substitutions

$$z \rightarrow z_c \zeta,$$

$$t \rightarrow t_c \tau,$$

$$\psi_i \rightarrow \psi_c \phi.$$

From here we will only consider the equation for the spin up component as the two will have the same non-dimensionalisation. After making these substitutions the above equation becomes

$$i\hbar \frac{\psi_c}{t_c} \partial_{\tau} \phi_{\uparrow} = -\frac{\hbar^2}{2m z_c^2} \partial_{\zeta\zeta} \phi_{\uparrow} - \frac{1}{2} \mu_B g_s dB_z z_c \zeta \psi_c \phi_{\uparrow} + \frac{1}{2} \mu_B g_s \psi_c B_x \phi_{\downarrow},$$

rearranging so that the coefficient of the highest derivative is dimensionless

$$i \frac{m z_c^2}{\hbar t_c} \partial_{\tau} \phi_{\uparrow} = -\frac{1}{2} \partial_{\zeta\zeta} \phi_{\uparrow} - \frac{1}{2} \frac{\mu_B g_s m dB_z z_c^3}{\hbar^2} \zeta \phi_{\uparrow} + \frac{1}{2} \frac{\mu_B g_s m z_c^2}{\hbar^2} B_x \phi_{\downarrow}.$$

From here we can see

$$z_c = \frac{B_x}{dB_z}, \quad (\text{E.13})$$

$$t_c = \frac{\hbar}{B_x g_s \mu_B}, \quad \text{1 / Larmor frequency around Bx} \quad (\text{E.14})$$

$$\psi_c = \frac{dB_z^2 \hbar^2}{B_x^3 g_s m \mu_B}. \quad (\text{E.15})$$

Leaving us with the non-dimensionalised equation

$$\partial_{\tau} \phi_{\uparrow} = \frac{1}{2} \partial_{\zeta\zeta} \phi_{\uparrow} + \frac{1}{2} \zeta \phi_{\uparrow} - \frac{1}{2} \phi_{\downarrow}.$$

More dummy text

LABITUR BONORUM PRI NO	QUE VISTA	HUMAN
fastidii ea ius	germano	demonstratea
suscipit instructor	titulo	personas
quaestio philosophia	facto	demonstrated

Table E.1: Autem usu id.

Listing E.1: A floating example

```

1 for i:=maxint to 0 do
  begin
    { do nothing }
  end;

```

### E.3 ANOTHER APPENDIX SECTION TEST

Curabitur tellus magna, porttitor a, commodo a, commodo in, tortor. Donec interdum. Praesent scelerisque. Maecenas posuere sodales odio. Vivamus metus lacus, varius quis, imperdiet quis, rhoncus a, turpis. Etiam ligula arcu, elementum a, venenatis quis, sollicitudin sed, metus. Donec nunc pede, tincidunt in, venenatis vitae, faucibus vel, nibh. Pellentesque wisi. Nullam malesuada. Morbi ut tellus ut pede tincidunt porta. Lorem ipsum dolor sit amet, consectetur adipiscing elit. Etiam congue neque id dolor.

Donec et nisl at wisi luctus bibendum. Nam interdum tellus ac libero. Sed sem justo, laoreet vitae, fringilla at, adipiscing ut, nibh. Maecenas non sem quis tortor eleifend fermentum. Etiam id tortor ac mauris porta vulputate. Integer porta neque vitae massa. Maecenas tempus libero a libero posuere dictum. Vestibulum ante ipsum primis in faucibus orci luctus et ultrices posuere cubilia Curae; Aenean quis mauris sed elit commodo placerat. Class aptent taciti sociosqu ad litora torquent per conubia nostra, per inceptos hymenaeos. Vivamus rhoncus tincidunt libero. Etiam elementum pretium justo. Vivamus est. Morbi a tellus eget pede tristique commodo. Nulla nisl. Vestibulum sed nisl eu sapien cursus rutrum.





## BIBLIOGRAPHY

---

- [1] G. A. Bird. Molecular Gas Dynamics and the Direct Simulation of Gas Flows. Clarendon, Oxford, 2 edition, 1994.
- [2] Huang Wu and Christopher J Foot. Direct simulation of evaporative cooling. Journal of Physics B: Atomic, Molecular and Optical Physics, (8):L321.
- [3] Huang Wu, Ennio Arimondo, and Christopher J. Foot. Dynamics of evaporative cooling for bose-einstein condensation. Phys. Rev. A, pages 560–569, Jul. doi:10.1103/PhysRevA.56.560.
- [4] Huang Wu and Ennio Arimondo. Expansion cooling for an atomic beam. Journal of Physics D: Applied Physics, 31(22):3218, 1998.
- [5] B. Jackson and C. S. Adams. Damping and revivals of collective oscillations in a finite-temperature model of trapped bose-einstein condensation. Phys. Rev. A, page 053606, Apr. doi:10.1103/PhysRevA.63.053606.
- [6] B. Jackson and E. Zaremba. Finite-temperature simulations of the scissors mode in bose-einstein condensed gases. Phys. Rev. Lett., page 100404, Aug. doi:10.1103/PhysRevLett.87.100404.
- [7] B. Jackson and E. Zaremba. Modeling bose-einstein condensed gases at finite temperatures with  $n$ -body simulations. Phys. Rev. A, page 033606, Sep. doi:10.1103/PhysRevA.66.033606.
- [8] B. Jackson and E. Zaremba. Quadrupole collective modes in trapped finite-temperature bose-einstein condensates. Phys. Rev. Lett., page 180402, Apr. doi:10.1103/PhysRevLett.88.180402.
- [9] B. Jackson and E. Zaremba. Accidental suppression of landau damping of the transverse breathing mode in elongated bose-einstein condensates. Phys. Rev. Lett., page 150402, Sep. doi:10.1103/PhysRevLett.89.150402.
- [10] Michael Urban and Peter Schuck. Dynamics of a trapped fermi gas in the bcs phase. Phys. Rev. A, page 013621, Jan. doi:10.1103/PhysRevA.73.013621.
- [11] Michael Urban. Coupling of hydrodynamics and quasiparticle motion in collective modes of superfluid trapped fermi gases. Phys. Rev. A, page 053607, May. doi:10.1103/PhysRevA.75.053607.
- [12] Michael Urban. Radial quadrupole and scissors modes in trapped fermi gases across the bcs phase transition. Phys. Rev. A, page 053619, Nov. doi:10.1103/PhysRevA.78.053619.

- [13] Thomas Lepers, Dany Davesne, Silvia Chiacchiera, and Michael Urban. Numerical solution of the boltzmann equation for the collective modes of trapped fermi gases. *Phys. Rev. A*, page 023609, Aug. doi:[10.1103/PhysRevA.82.023609](https://doi.org/10.1103/PhysRevA.82.023609).
- [14] P. Vignolo, M.L. Chiofalo, M.P. Tosi, and Sauro Succi. Explicit finite-difference and particle method for the dynamics of mixed bose-condensate and cold-atom clouds. *Journal of Computational Physics*, (2):368 – 391. doi:<http://dx.doi.org/10.1006/jcph.2002.7171>.
- [15] F. Toschi, P. Vignolo, S. Succi, and M. P. Tosi. Dynamics of trapped two-component fermi gas: Temperature dependence of the transition from collisionless to collisional regime. *Phys. Rev. A*, page 041605, Apr. doi:[10.1103/PhysRevA.67.041605](https://doi.org/10.1103/PhysRevA.67.041605).
- [16] P. Capuzzi, P. Vignolo, F. Toschi, S. Succi, and M. P. Tosi. Effects of collisions against thermal impurities in the dynamics of a trapped fermion gas. *Phys. Rev. A*, page 043623, Oct. doi:[10.1103/PhysRevA.70.043623](https://doi.org/10.1103/PhysRevA.70.043623).
- [17] F. Toschi, P. Capuzzi, S. Succi, P. Vignolo, and M. P. Tosi. Transition to hydrodynamics in colliding fermion clouds. *Journal of Physics B: Atomic, Molecular and Optical Physics*, (7):S91. doi:[10.1088/0953-4075/37/7/056](https://doi.org/10.1088/0953-4075/37/7/056).
- [18] P. Barletta, J. Tennyson, and P. F. Barker. Direct monte carlo simulation of the sympathetic cooling of trapped molecules by ultracold argon atoms. *New Journal of Physics*, (11):113002. doi:[10.1088/1367-2630/12/11/113002](https://doi.org/10.1088/1367-2630/12/11/113002).
- [19] Paolo Barletta. Cool: A code for dynamic monte carlo simulation of molecular dynamics. *Computer Physics Communications*, (2):388 – 399. doi:<http://dx.doi.org/10.1016/j.cpc.2010.09.015>.
- [20] Tadashi Watanabe, Hideo Kaburaki, and Mitsuo Yokokawa. Simulation of a two-dimensional rayleigh-bénard system using the direct simulation monte carlo method. *Phys. Rev. E*, pages 4060–4064, May. doi:[10.1103/PhysRevE.49.4060](https://doi.org/10.1103/PhysRevE.49.4060).
- [21] E.S. Oran, C.K. Oh, and B.Z. Cybyk. DIRECT SIMULATION MONTE CARLO: recent advances and application. *Annual Review of Fluid Mechanics*, 30:403–441, 1998.
- [22] James B. Anderson and Lyle N. Long. Direct monte carlo simulation of chemical reaction systems: Prediction of ultrafast detonations. *The Journal of Chemical Physics*, 118(7), 2003.
- [23] Attilio Frangi, Carlo Cercignani, Subrata Mukherjee, and Narayan Aluru. *Advances in Multiphysics Simulation and Experimental Testing of MEMS*. Imperial College Press, London, 2008.



- [24] Amanda D. Hanford and Lyle N. Long. The direct simulation of acoustics on earth, mars, and titan. The Journal of the Acoustical Society of America, 125(2), 2009.
- [25] Numerical modeling of ionian volcanic plumes with entrained particulates. Icarus, 172(2):479 – 502, 2004. doi:<http://dx.doi.org/10.1016/j.icarus.2004.06.016>.
- [26] A. Minguzzi, S. Succi, F. Toschi, M.P. Tosi, and P. Vignolo. Numerical methods for atomic quantum gases with applications to bose–einstein condensates and to ultracold fermions. Physics Reports, (4–5):223 – 355. doi:<http://dx.doi.org/10.1016/j.physrep.2004.02.001>.
- [27] Jook T Walraven. Elements of Quantum Gases: Thermodynamic and Collisional Properties of Trapped Atomic Gases. University of Amsterdam, 2010.
- [28] M. Anderlini and D. Guéry-Odelin. Thermalization in mixtures of ultracold gases. Phys. Rev. A, 73:032706, Mar 2006. doi:[10.1103/PhysRevA.73.032706](https://doi.org/10.1103/PhysRevA.73.032706).
- [29] Christopher John Myatt. Bose-Einstein Condensation Experiments in a Dilute Vapor of Rubidium. PhD thesis, University of Colorado, 1997.
- [30] C. R. Monroe, E. A. Cornell, C. A. Sackett, C. J. Myatt, and C. E. Wieman. Measurement of cs-cs elastic scattering at  $t=30\text{ }\mu\text{k}$ . Phys. Rev. Lett., 70:414–417, Jan 1993. doi:[10.1103/PhysRevLett.70.414](https://doi.org/10.1103/PhysRevLett.70.414).
- [31] Kendall B. Davis, Marc-Oliver Mewes, Michael A. Joffe, Michael R. Andrews, and Wolfgang Ketterle. Evaporative cooling of sodium atoms. Phys. Rev. Lett., 74:5202–5205, Jun 1995. doi:[10.1103/PhysRevLett.74.5202](https://doi.org/10.1103/PhysRevLett.74.5202).
- [32] O. J. Luiten, M. W. Reynolds, and J. T. M. Walraven. Kinetic theory of the evaporative cooling of a trapped gas. Phys. Rev. A, 53:381–389, Jan 1996. doi:[10.1103/PhysRevA.53.381](https://doi.org/10.1103/PhysRevA.53.381).
- [33] M Holland, J Williams, K Coakley, and J Cooper. Trajectory simulation of kinetic equations for classical systems. Quantum and Semiclassical Optics: Journal of the European Optical Society Part B, 8(3):571.
- [34] Bemerkung über die angenäherte gültigkeit der klassischen mechanik innerhalb der quantenmechanik. Zeitschrift für Physik, 45(7-8), 1927. doi:[10.1007/BF01329203](https://doi.org/10.1007/BF01329203).
- [35] Loup Verlet. Computer "experiments" on classical fluids. i. thermodynamical properties of lennard-jones molecules. Phys. Rev., pages 98–103, Jul. doi:[10.1103/PhysRev.159.98](https://doi.org/10.1103/PhysRev.159.98).

- [36] R W Hockney. The potential calculation and some applications. Methods in Computational Physics, 9:136–211, 1970.
- [37] William C. Swope, Hans C. Andersen, Peter H. Berens, and Kent R. Wilson. A computer simulation method for the calculation of equilibrium constants for the formation of physical clusters of molecules: Application to small water clusters. The Journal of Chemical Physics, (1):637–649. doi:<http://dx.doi.org/10.1063/1.442716>.
- [38] D. Beeman. Some multistep methods for use in molecular dynamics calculations. Journal of Computational Physics, (2):130 – 139. doi:[http://dx.doi.org/10.1016/0021-9991\(76\)90059-0](http://dx.doi.org/10.1016/0021-9991(76)90059-0).

## COLOPHON

This document was typeset using the typographical look-and-feel `classicthesis` developed by André Miede. The style was inspired by Robert Bringhurst's seminal book on typography "The Elements of Typographic Style". `classicthesis` is available for both  $\text{\LaTeX}$  and  $\text{\LyX}$ :

<http://code.google.com/p/classicthesis/>

Happy users of `classicthesis` usually send a real postcard to the author, a collection of postcards received so far is featured here:

<http://postcards.miede.de/>



## DECLARATION

---

Put your declaration here.

*Clayton, Victoria, December 2013*

---

Christopher Jon Watkins,  
December 18, 2014